

Extended-Range Linear Magnetostrictive Motor With Double-Sided Three-Phase Stators

Won-Jong Kim, *Member, IEEE*, James H. Goldie, Michael J. Gerver, Jerome E. Kiley, and John R. Swenbeck

Abstract—The authors have developed a novel extended-range linear magnetostrictive motor using the peristaltic motion of a laminated Terfenol-D ($Tb_{0.3}Dy_{0.7}Fe_2$) element. This element migrates in the opposite direction of the traveling magnetic field generated by prevailing three-phase armature commutation. The actuator mechanical design is in an open structure in order to allow easy assembly and access to internal actuator components. Eight sets of Belleville washers guarantee uniform squeeze preload in spite of wear, thermal expansion, or motion of the moving element. We incorporated a laminated Terfenol-D slab in this actuator to reduce the eddy current, leading to high-frequency high-speed operation. We have also designed and constructed the power electronics and control units for the magnetostrictive actuator's open-loop and closed-loop operations. With a series-resonant capacitor, we were able to achieve a near-unity power factor and decrease the reactive power requirement by a factor of 20. The magnetostrictive motor has demonstrated 12-mm/s speed at excitation frequency of 1600 Hz, and shown 140-N load capacity. The effective travel range of the present motor is 25 mm, and can be extended further. This linear magnetostrictive motor shows great potential in high-force precision positioning applications such as automotive actuators, robotics, and flight control surface actuators.

Index Terms—Automotive actuator, linear motor, magnetostriction, magnetostrictive actuator, real-time digital control, robotics, three-phase motor.

I. INTRODUCTION

RESEARCHERS are seeking to develop electrically-powered actuators that can provide greater forces and torques within a given volume. In particular, if electric actuators can achieve force (or torque) densities which are comparable with hydraulic actuators, then there are a wide range of potential applications of electric actuation in high-force precision positioning systems: robotics, automated manufacturing, flight or naval control surface actuators, appliances, pump drives, and so forth. Furthermore, a future market in the automotive business is developing because of the increasing interest in electric

Paper IPCSD 01-082, presented at the 1999 Industry Applications Society Annual Meeting, Phoenix, AZ, October 3-7, and approved for publication in the IEEE TRANSACTIONS ON INDUSTRY APPLICATIONS by the Electric Machines Committee of the IEEE Industry Applications Society. Manuscript submitted for review May 1, 2000 and released for publication January 24, 2002. This work was supported by the National Aeronautics and Space Administration under Grant C NAS9-97006.

W.-J. Kim is with the Department of Mechanical Engineering, Texas A&M University, College Station, TX 77843-3123 USA (e-mail: wjkim@mengr.tamu.edu).

J. H. Goldie, J. E. Kiley, and J. R. Swenbeck are with SatCon Technology Corporation, Cambridge, MA 02142 USA (e-mail: goldie@satc.com; kiley@satc.com; swenbeck@satc.com).

M. J. Gerver is with Fenster & Company, Petach-Tikvah, Israel (e-mail: mjgerver@aol.com).

Publisher Item Identifier S 0093-9994(02)04500-0.

and hybrid electric vehicles. In addition to providing traction for these vehicles, electric actuators and motors will be the natural choice for all auxiliary functions such as power steering, air conditioning compressor drives, brakes, and even automatic transmissions. Since direct-drive electric linear motors fail to match the force capability of hydraulics, rotary motors have been combined with gear reducers and ball or lead screws to create a high force linear actuator. This approach, although effective in many situations, requires the added complexity of a speed reducer and introduces backlash. Moreover, it may be too sluggish for applications requiring rapid response and maneuvering.

In response to these limitations, we have been developing novel linear and rotary electric machines which employ Terfenol-D ($Tb_{0.3}Dy_{0.7}Fe_2$), a giant magnetostrictive material introduced by the Naval Ordnance Laboratory, in a configuration in which it travels like an inchworm along a channel with tight-fitting walls [1], [2]. The result is a device which combines extended travel with the well-known high force and torque capability of magnetostrictive actuation. Furthermore, the motor self-brakes and holds its position when unpowered, which is beneficial to many applications. These magnetostrictive actuators do not require bearings or other components with friction, suggesting their utility in precision positioning applications.

This approach has been implemented with piezoelectrics to overcome their limited micrometer-order travel range for low-force high-precision positioning. For higher force applications, there has been research over the last decade into the development of a variety of magnetostrictive devices. Kiesewetter at the Technical University of Berlin demonstrated peristaltic action with a cylinder of Terfenol in a tight-fitting tube in the late 1980s [3]. After Kiesewetter, there were several notable research results on actuation with magnetostrictive materials. Vranish *et al.* designed a magnetostrictive rotary motor using Terfenol-D [4]. Wang and Busch-Vishniac devised a two-dimensional micropositioner by conjugating two linear magnetostrictive actuators [5]. Claeysen *et al.* built a high-torque motor using magnetostriction and resonance effects of Terfenol-D [6]. Teter *et al.* addressed electromechanical modeling issues of a magnetostrictive linear motor [7]. A recent survey paper presents development of Terfenol-D and their applications for smart air vehicles [8].

We have conceived of a means by which a laminated Terfenol-D element is excited with prevailing polyphase windings. Fig. 1 shows such a magnetostrictive motor we developed. Unlike Kiesewetter's cylindrical design or any other configurations that followed, the Terfenol-D element in our design is a rectangular slab placed between two tight-fitting plates that are spring loaded to maintain proper contact in spite of wear, thermal ex-

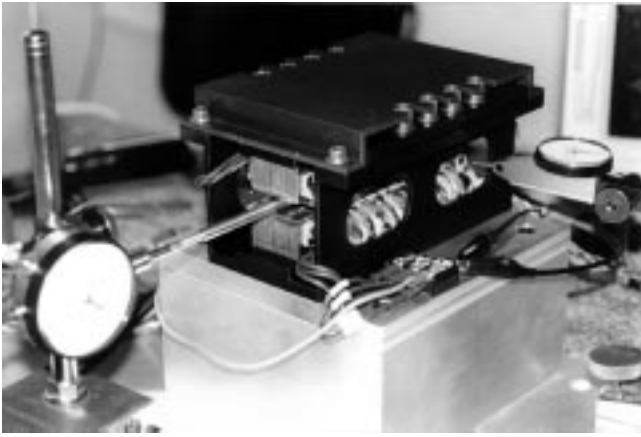


Fig. 1. Photograph of the extended-range linear magnetostrictive motor with double-sided three-phase stators.

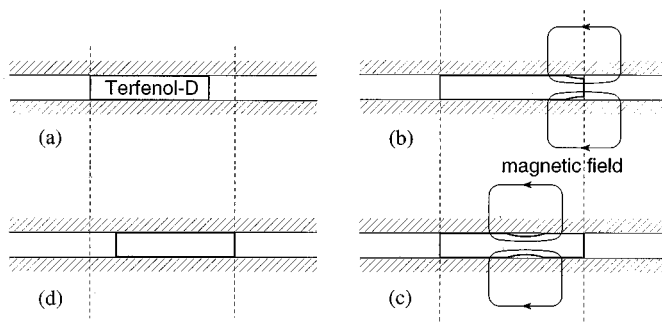


Fig. 2. Working principle of the linear magnetostrictive actuator. The sandwiched magnetostrictive element migrates in the opposite direction of the traveling magnetic field generated by the commutation in the armatures. Clockwise from the upper left corner: part (a) initial position; part (b) initial field interaction; part (c) field propagation; and part (d) final displaced position.

pansion, or motion. Contrary to piezoelectric peristaltic actuators, our magnetostrictive motor shows a smooth and continuous motion. We demonstrated speed of 12 mm/s at 1600-Hz excitation frequency, and 140-N load capacity with this magnetostrictive motor. In addition, we looked at ways to address the major challenges associated with this type of device: low power factor and high eddy-current losses. This paper describes how the actuator is configured, how it works, how it solves the challenges, theoretical predictions of its performance, power and control electronics, and experimental results.

In the next section, we present the working principle and the electromagnetic design of the extended-range linear magnetostrictive motor. Its mechanical design and fabrication are described in Section III. Open-loop and closed-loop test results of the motor are provided in the following sections. In conjunction with the test results, a detailed description on the power and control electronics are presented.

II. WORKING PRINCIPLE AND ELECTROMAGNETIC DESIGN

The principle of operation of a linear magnetostrictive motor is shown in Fig. 2. The unpowered condition is depicted in (a) of the figure, where a length of magnetostrictive element with rectangular cross section is confined to the channel between two stationary planar surfaces. When no magnetic fields are applied to the element, there exists a tight fit between the channel and

the element. This static squeeze preloading produces the normal force necessary for fail-safe joint locking. Parts (b) and (c) of Fig. 2 show the effects of a swept longitudinal magnetic field on the shape and location of the magnetostrictive element. The field lines are oriented as shown and are swept from right to left. As the field begins to interact with the element [part (b)], that portion of the element expands along the field lines, extending to the right. As the field passes completely into the element, the right portion of the element returns to its original shape, locking against the channel [part (c)]. As the field continues through the element, the extended region propagates through the block until the field passes completely to the left. The element has effectively moved to the right, while simultaneously maintaining contact with the channel.

A. Underlying Theory

We have analyzed the actuator (for force or torque, speed, and losses) as a function of the design parameters and applied electrical power previously [9]. This analysis included the effect of the compressibility of the Terfenol-D slab. It produced important conclusions, regarding the speed capability of the device. Neglecting the effect of the finite contact area between the Terfenol and the channel, the analysis showed that the output speed (v) of the magnetostrictive motor is given by

$$v = \frac{\omega}{k} \left(\epsilon_{\max} - \frac{F}{EA_T} \right), \quad (1)$$

where

- ω temporal frequency (rad/s) of stress, strain, and displacement in the Terfenol-D ($=2 \times$ electrical excitation frequency);
- k wave number ($2\pi/\text{pole pitch}$), where the pole pitch is 28.8 mm ($=218 \text{ m}^{-1}$);
- ϵ_{\max} peak magnetostrictive strain under no-load condition;
- E Young's modulus of Terfenol-D ($=50 \text{ GPa}$);
- F external load (N);
- A_T cross-sectional area of the Terfenol-D ($=9.5 \text{ mm} \times 28.0 \text{ mm} = 266 \times 10^{-6} \text{ m}^2$).

Note that ω/k equals the propagation of phase velocity of the excitation field. F/EA_T is the load-induced strain in the Terfenol-D cross section. Thus, F/EA_T reduces or increases the no-load magnetostriction ϵ_{\max} , depending on the direction of the external load F . It accounts for extension or contraction of the Terfenol-D slab under the influence of the external load.

If there is no external load, the speed of the Terfenol-D element is equal to the product of the extensional growth of each of the regions of the Terfenol-D element that have drawn away from the stator plates and the number of these regions that pass per unit time. This is equal to the product of the phase velocity of the sinusoidal field pattern and the magnetostrictive strain

$$v = \frac{\omega}{k} \epsilon_{\max}. \quad (2)$$

B. Optimized Motor Parameters

We performed design optimization for the Terfenol-D, pole, back iron, and slot dimensions to generate the best performance in the smallest actuator dimension and power consumption.

TABLE I
OPTIMIZED PARAMETERS FOR THE MAGNETOSTRICTIVE MOTOR

Terfenol-D element dimension	9.5 × 28.0 × 57.6 mm
phase resistance	0.45 Ω
phase inductance	0.78 mH
number of phases	3
number of coils per phase per stator	4
number of turns per coil	36
wire size (wound four in hand)	AWG #27
number of slots per stator	14
slot pitch	9.6 mm
pole pitch	3 slots
coil pitch	2 slots

A coil consists of 36 turns of four-in-hand AWG #27 wire because of the greater flexibility of the thinner wire that made the stator easier to wind. There are four such coils connected in series in a phase for each of the upper and lower stators, and the windings are double layered with a 2/3 pole pitch. The inductance and the resistance of the stator phase windings are 0.78 mH and 0.45 Ω with the stators connected in parallel. Table I summarizes the optimized parameters for the linear magnetostrictive motor.

C. Lamination of Terfenol-D

We obtained two laminated Terfenol-D slabs and a monolithic slab for testing of the magnetostrictive motor from Etrema Products, Inc., Ames, IA. According to the manufacturer's test report, the maximum strain in the laminated Terfenol-D slab is 1100 ppm at 140-kA/m magnetic field, and the surface finish of the slabs is 0.75 μm. As a rare-earth ferroalloy, Terfenol-D is a fair electric conductor; its resistivity is $\rho = 6.0 \times 10^{-7}$ Ω·m [10]. Using the permeability of the Terfenol-D, $\mu = 9\mu_0$ (where μ_0 is the permeability of free space, $4\pi \times 10^{-7}$ H/m), the skin depth at 2-kHz excitation frequency is $\delta = \sqrt{2\rho/\omega\mu} = 3$ mm. Thus, significant performance degradation is expected with monolithic Terfenol-D at high excitation frequency as the thickness of the Terfenol-D slab is 9.5 mm. We designed the lamination thickness at 2 mm, based on consideration of the maximum operating frequency of 2 kHz and mechanical integrity concerns [10]. Initial testing indicated that we could run the magnetostrictive actuator with the laminated Terfenol slab at the excitation frequency up to 2 kHz. The skin effect prevented the monolithic Terfenol slab from operating beyond the excitation frequency. Furthermore, the monolithic slab overheated at 400 Hz, due to eddy-current loss. All the experimental results presented in this paper were obtained with the laminated Terfenol-D slab. Very recent research by Stillesjö *et al.* deals with general design issues with laminated magnetostrictive materials [11].

III. MECHANICAL DESIGN AND FABRICATION

The mechanical design tasks of the linear magnetostrictive motor involved the design of suitable housing, transmission, and stator preload components. A test stand was also designed and built. We have designed two versions of the linear actuator: a

moving and a stationary Terfenol-D element actuator. In the moving Terfenol-D version presented in this paper, there is a stator above and below the Terfenol-D element. This improves performance for a given field in that the field is more symmetric with respect to a horizontal plain in the middle of the Terfenol-D element. In addition, it reduces the amount of leakage flux.

A. Moving Terfenol Design

The motor design, shown in Fig. 3, is characterized by a traveling active element, which is the Terfenol-D component that produces motion in the motor. The Terfenol-D slab is sandwiched between two linear stators, which are capped with thin pieces of Inconel-718 (indicated as stator intermediary plates in Fig. 3) that provide appropriately stiff surfaces against which the Terfenol-D element may act. Each stator intermediary plate has three thin grooves to reduce eddy-current loss. The friction forces between the stationary armatures and the Terfenol-D element provide the reaction force required to move the active element against a load or to hold it in place. A preload applied to the stators develops these friction forces. This preload is transmitted through a preload plate by the use of Belleville spring washers and bolts. These spring washers also provide a stiffness that is low enough to allow the Terfenol-D element to grow appropriately against the stators. The housing provides a spacious, rigid support, as well as a clear view into the motor.

B. Preloading Design

A squeeze preload is required to produce friction forces at the patches of contact between the Terfenol-D element and the intermediary plates on the stators. Ideally, this preload would be applied at exactly the same lengthwise locations as those where the contact patches occur. A satisfactory and practical solution is to use linear stiffness elements at discrete locations. The translational stiffness should ideally be zero (so that the transverse loading on the active element always remains the same), and the rotational stiffness should be infinite. We considered using a flexure-based design for preloading, as well as a Belleville-washer-based design. We found that we could obtain the same rotational stiffness using six or eight discrete spring locations as those obtained with a continuous, distributed stiffness like that exhibited by a flexure. We chose to use the Belleville-washer approach because of its higher adjustability and durability and its lower cost and complexity. The Belleville washers are expected to provide a net translational stiffness of 1750 N/mm and a preload of about 890 N, which is required based on an estimated coefficient of friction between Terfenol-D and Inconel-718 of 0.3 and a maximum motor load of 267 N.

C. Testing Subassembly

The testing subassembly is shown in Fig. 4. The major parts of the testing subassembly are the motor, the load, the transmission, a linear variable differential transformer (LVDT), and a mounting plate. The load and the transmission are made up of several subcomponents, and there are also mounting blocks to raise the height of the motor to match the height of the center of mass of the load. We have completed the design of a test stand

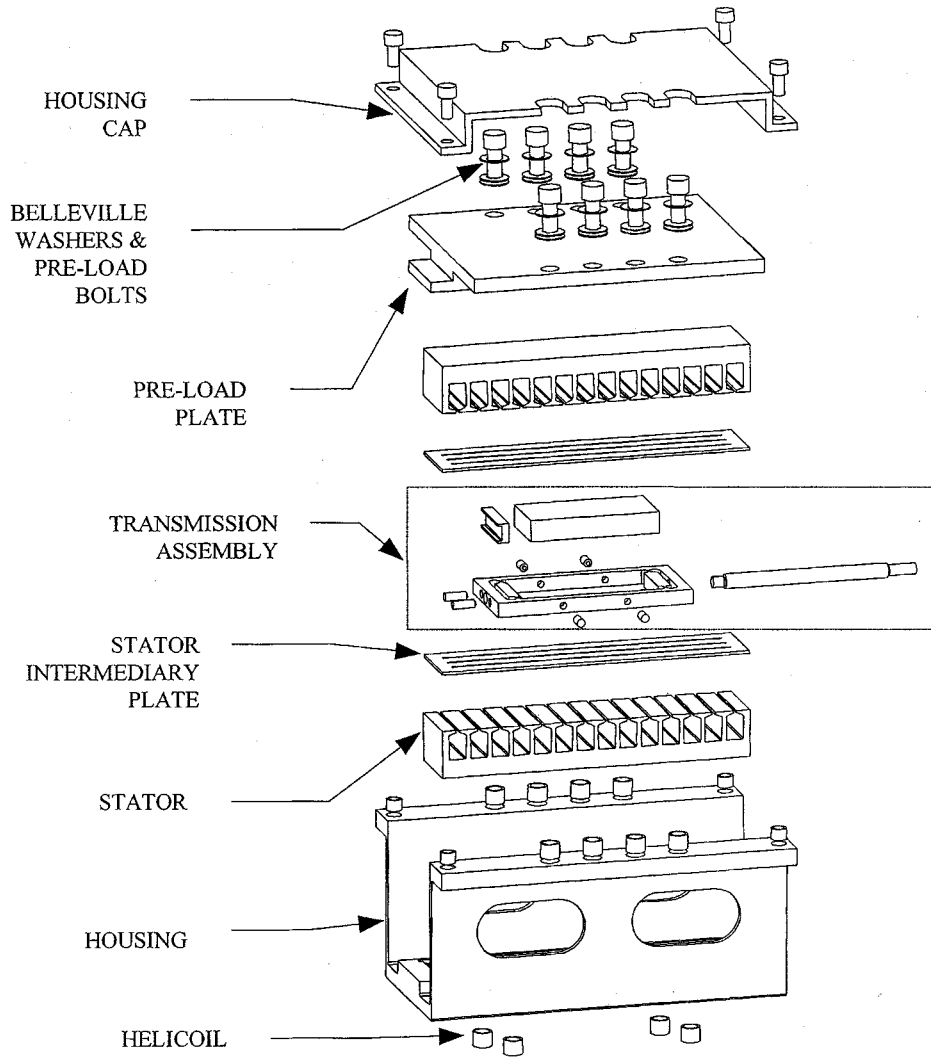


Fig. 3. Exploded view of the motor components. Two stators and the active Terfenol-D element inside the transmission assembly are shown.

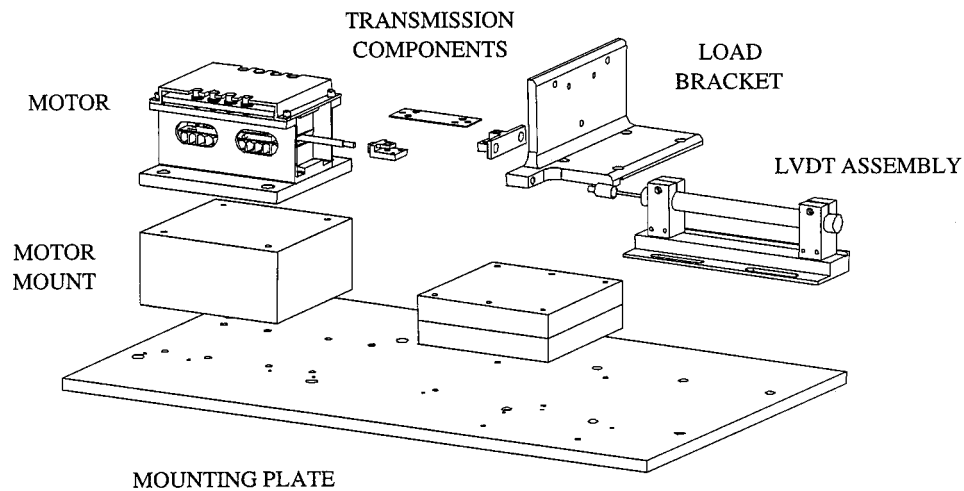


Fig. 4. Testing subassembly. This subassembly is ultimately mounted to a test stand for no-load and load tests.

that will allow us to orient the actuator either vertically or on a 30° slope. This allows us to load it with a combination of inertial and deadweight loads.

IV. POWER ELECTRONICS AND OPEN-LOOP TESTS

This section presents test results with the laminated Terfenol-D element including open-loop no-load and load tests

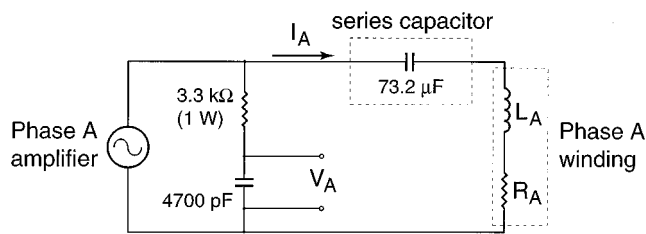


Fig. 5. Circuit for PFC.

under various operating conditions. We have also designed and constructed power and control electronics for the motor. Due to its inductive nature, a magnetostrictive motor requires rather large reactive power for its operation. We implemented a power-factor-correction (PFC) scheme, and present its experimental verification in this section.

A. Power and Control Electronics

The drive electronics for the actuator must be able to generate variable-voltage/frequency three-phase power to excite the actuator's stator windings. The power electronics and control system consists of the following components: a three-phase pulsewidth modulation (PWM) power amplifier that generates the required output power, an input isolation transformer/line rectifier to generate the required dc input power, and a digital signal processor (DSP) board to implement control and input functions. Actuator position feedback is provided through an LVDT position transducer.

The stator is in a floating neutral (six lead) configuration, and three commercial servo amplifiers provide the ac power for each phase. The amplifiers (model 25A20T by Advanced Motion Controls) are mounted on an air-cooled heat sink. The amplifiers require an analog reference signal and can be configured as either closed-loop voltage or current sources. DC input power is generated by a full-wave rectifier assembly consisting of a 220-V input/110-V output isolation transformer, an SCR relay (to remove input ac line power), and a full-wave diode bridge. A 10 000-mF capacitor is included for filtering.

The servo amplifier reference signals and control functions are implemented in a Sat32 DSP board developed previously by SatCon Technology Corporation, Cambridge, MA. The system has a 32-bit 60-MHz floating-point DSP (TMS320C32 by Texas Instruments), with eight analog inputs, eight analog outputs, and 16 digital I/O channels. The reference sine waves for commutation are stored in a lookup table (in on-board memory), and the feedback controller is implemented digitally.

B. PFC

The circuit for the PFC is shown in Fig. 5. The 3.3-k Ω /4700-pF filter was used to remove the 20-kHz PWM ripple component of the power amplifiers' output voltage. The cutoff frequency for the filter is 10 kHz, which provided some attenuation of the ripple component but allowed the signal up to 2 kHz to pass with essentially no phase lag. Voltage and current traces for phase A at 470 Hz are shown in Fig. 6. Without

correction, a power factor of 0.352 is observed in Fig. 6(a). When a 73.2- μ F series capacitor is included, the power factor is 0.989, achieving the goal of near-unity power factor. Of even greater significance is the reduction in the applied phase voltage. The peak phase voltage in Fig. 6(a) is 27.7 V. This is reduced to 8.55 V with the series capacitor. Since both tests were done with a 5-A peak current, a 69.2% reduction in the V-A output of the amplifier is achieved. A similar reduction is shown at 650 Hz, where the peak voltage was reduced by 61.8%, from 32.9 to 20.3 V.

At all frequencies tested, the inclusion of the series capacitor reduced the reactive power required to source the motor phase current. Note in particular that a significant reduction in reactive power is achieved at the resonant frequency of 470 Hz, from 130 to 6 var. The PFC test results at three representative operating frequencies are tabulated in Table II.

C. Open-Loop No-Load and Load Tests

We performed open-loop no-load tests under various operating conditions by changing squeeze preload, and phase voltage and current. In these open-loop tests, the two stators were connected in series. Fig. 7 shows such an open-loop motion profile at excitation frequency of 1600 Hz under no-load condition. The phase voltage and current are 300 V and 6 A, respectively. The motor slows down significantly after the 15-mm mark, because it is now out of its travel range and does not generate sufficient field for the peristalsis of the Terfenol-D slab.¹ This plot demonstrates a 12-mm/s speed capability of the linear magnetostrictive motor.

To show the motor performance dependency on phase voltage and current, Fig. 8 presents a set of the Terfenol-D motion profiles at excitation frequency of 400 Hz with 360-N squeeze preload. Increasing phase voltage and current increases speed as predicted by theory. We find that at least 4.2-A phase current is required to move the Terfenol-D slab. The implications of this threshold current were a sizeable dead zone and significant ohmic loss, even at low speed when operating under current control. We found that we could lower this threshold by lapping the contacting surfaces of the stator and Terfenol-D element to improve flatness. This dead-zone effect is discussed fully in Section V.

Following the no-load tests, we performed open-loop load tests under various operating conditions. The motor components on the mounting plated shown in Fig. 4 were mounted on a 30° slope. Fig. 9 shows a set of the Terfenol-D motion profiles with 720-N squeeze preload at excitation frequency of 400 Hz, with varying load. The corresponding phase voltage and current are 75 V and 5 A, respectively. Weights including the load bracket are imposed on the same 30° slope. The reported load is the component of the weight vector along the direction of motion. As shown in Fig. 9, the motor speed is inversely related to the external load. We observed noticeable Terfenol-D motion with 140-N load, 720-N preload, and an excitation at 400 Hz with phase voltage and current of 120 V and 10.5 A.

¹Recall that the travel range of the present magnetostrictive motor is ± 12.5 mm. The Terfenol-D slab was located at the center of the range initially.

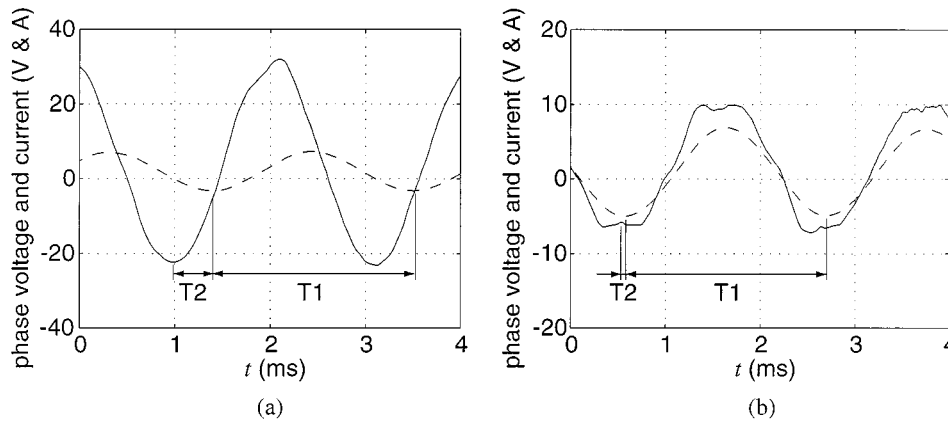


Fig. 6. PFC test results at excitation frequency of 470 Hz, showing phase current (dashed) and voltage (solid) traces. (a) Without PFC ($T_1 = 2.128$ ms, $T_2 = 410.3$ μ s, power factor = 0.352). (b) With PFC ($T_1 = 2.128$ ms, $T_2 = 51.3$ μ s, power factor = 0.989).

TABLE II
SUMMARY OF POWER-FACTOR-CORRECTION TEST RESULTS

freq. (Hz)	PFC	phase angle	power factor	phase volt. (peak)	reactive power
400	no	70.2°	0.339	23.6 V	111 VAR
400	yes	-66.5°	0.400	12.9 V	59.2 VAR
470	no	69.4°	0.352	27.7 V	130 VAR
470	yes	8.68°	0.989	8.55 V	6.45 VAR
650	no	60.0°	0.500	32.9 V	143 VAR
650	yes	51.0°	0.630	20.3 V	79.0 VAR

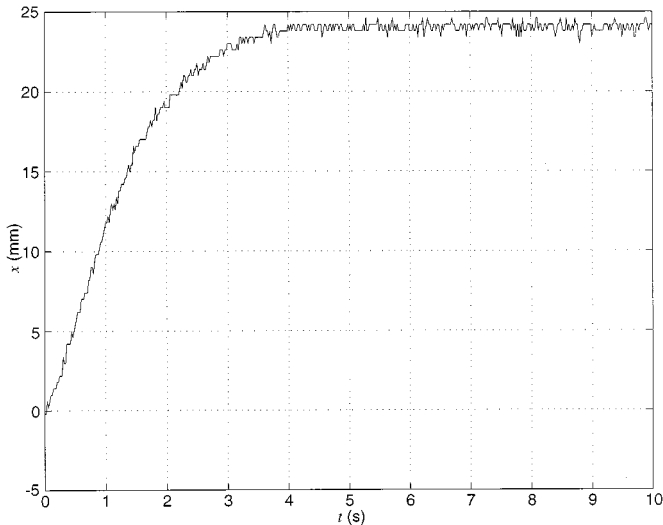


Fig. 7. Open-loop motion profile at excitation of 1600 Hz under no-load condition. The phase voltage and current are 300 V and 6 A, respectively. It shows 12-mm/s speed capability of the linear magnetostrictive motor.

V. CLOSED-LOOP TESTS

A. Control Strategies

We use the simplified no-load speed model (2) in Section II for control development. The magnetostrictive strain (ϵ_{\max}) can be represented as a multiplication of a peak phase current and a scale factor that can be determined experimentally. This scale factor k_ϵ varies with respect to the peak phase current (i), temporal frequency (ω), and squeeze preload, load, etc. For instance, $k_\epsilon = 6.06 \times 10^{-6} \text{ A}^{-1}$ with 10.5-A phase current, 400-Hz excitation frequency, with 360-N squeeze preload

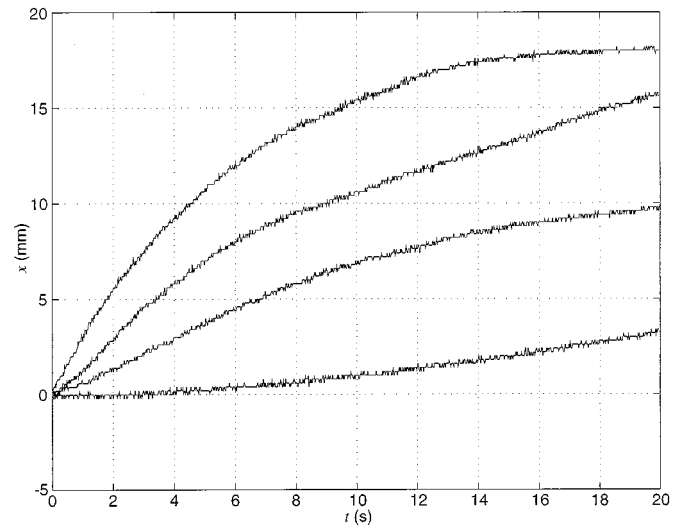


Fig. 8. Open-loop motion profiles with 360-N squeeze preload at excitation of 400 Hz under no-load condition, varying phase voltage, 120, 100, 80, and 60 V from the top. The phase currents are 10.5, 8.2, 6.0, and 4.2 A, respectively.

under no-load condition. This speed model gives a good insight into the magnetostrictive motor operation. However, an accurate model is hard to obtain because of the model uncertainties and nonlinearities including dead zone, hysteresis, slip, surface conditions, thermal expansion, and the like. Later in this section, we present successful closed-loop control test results after tuning the controller with various combinations of proportional and integral gains.

Since the speed is dependent on both current and frequency, two different controllers can be implemented. The first controller holds the frequency constant and varies the amplitude of the phase current as the control input (the current control scheme). The second controller holds the phase current amplitude constant and varies the frequency as the control input (the frequency control scheme). Both the controllers use proportional-integral (PI) control. The motor position is measured by an LVDT (2000 DC-SE by Schaevitz). The maximum sensing range of the LVDT is ± 25 mm and its sensitivity is 10 mm/V. The output of the LVDT is read into the computer and compared to the commanded position. The error signal is operated on by the controller, resulting in a current or frequency command. Using lookup tables, the DSP generates balanced three-phase

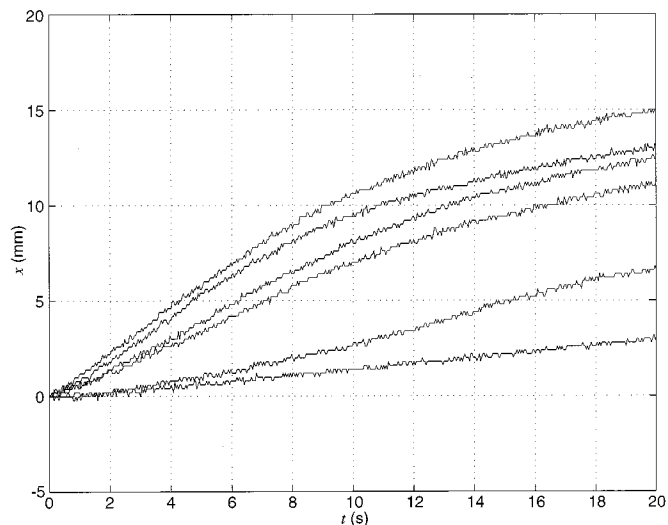


Fig. 9. Open-loop motion profiles with 720-N squeeze preload at excitation of 400 Hz, varying load, 11, 22, 33, 44, 66, and 77 N from the top. The phase voltage and current are 75 V and 5 A, respectively.

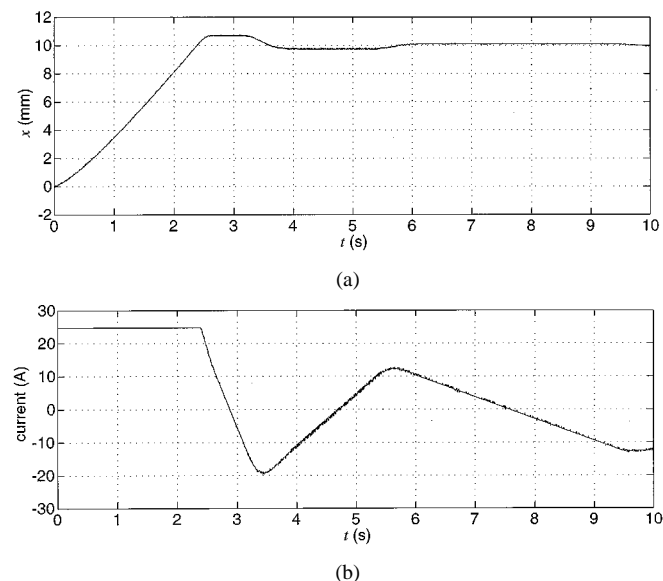


Fig. 10. 10-mm closed-loop step response and its corresponding current input with PI current control with the fixed excitation frequency of 800 Hz.

sine waves with the commanded amplitude and frequency. The sine waves are output via digital-to-analog converters to the PWM amplifiers that establish current in the windings. The sampling rate of the control system is 20 kHz, and the bandwidth of the antialiasing filter and the smoothing filter is set at 3 kHz. The stators of the motor are connected in parallel, and the PFC scheme in Section IV is employed in the experiments.

B. Step Responses With Current Control

Fig. 10(a) shows a closed-loop step response under no-load condition with the current control scheme. The step command is 10 mm and the excitation frequency is fixed at 800 Hz. The proportional gain K_P is 40 A/m, and the integral gain K_I is 256 A/m·s. Fig. 10(b) shows the corresponding phase current input to the magnetostrictive motor. The phase current is saturated at 25 A by the power amplifier rating in the beginning. In

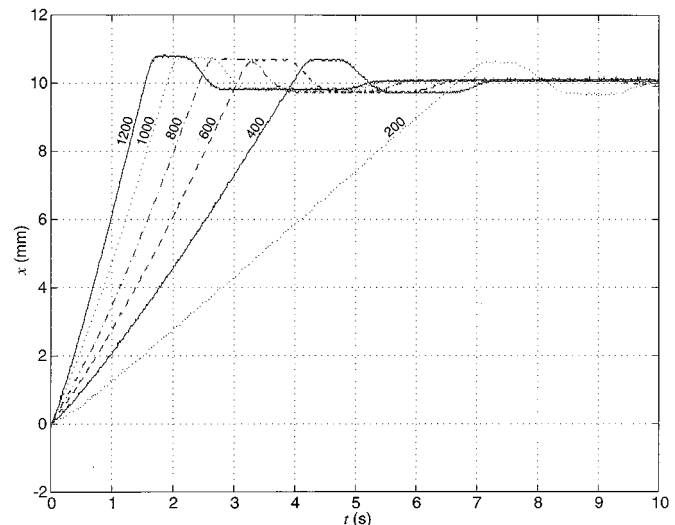


Fig. 11. 10-mm closed-loop step responses with current PI control with fixed excitation frequencies of 1200, 1000, 800, 600, 400, and 200 Hz from the left.

this test result and the following, we implemented an integrator antiwindup scheme, and the error integration limit is set at 1 A [12]. Fig. 11 shows step responses with the current control, for various excitation frequencies from 200 to 1200 Hz with the same PI controller. As expected in our theory, the initial (saturation) speed of the motor is proportional to the frequency with all the other conditions fixed.

One thing to note for this current control test results is that the trajectories shown in Figs. 10 and 11 have “plateaus” during the settling oscillations from the integration action of the controller. These plateaus resulted from the current input dead zone presently of 4.2 A that is inherent in the class of magnetostrictive motors. In other words, the motor would not correct a position error by reversing its direction until the controller accumulates enough error signal to overcome the dead zone. This phenomenon is not as prominent in the frequency control cases, as in Fig. 12, since there is little, if any, dead zone in the frequency control scheme.

C. Step Response With Frequency Control

Fig. 12(a) shows a closed-loop step response under no-load condition with the frequency control scheme. The step command is 10 mm and the phase current is fixed at 25 A. The proportional gain K_P is 40 Hz/m, and the integral gain K_I is 256 Hz/m·s. Fig. 12(b) shows the corresponding frequency input to the magnetostrictive motor. The frequency input is limited at 1200 Hz in the beginning to ensure proper operation in high frequency.

Provided that the two control schemes show similar dynamic performances in terms of settling time, rise time, overshoot, etc., the frequency control seems favorable in a sense that the speed of the motor linearly depends on the frequency at a fixed current magnitude by the theory. In addition, the frequency control scheme does not exhibit the dead zone that is significant in the current control scheme. One downside of the frequency control scheme is that the motor consumes significant power even after the commanded position has been reached. The power source can be turned off when the position error is reduced under a predetermined bound.

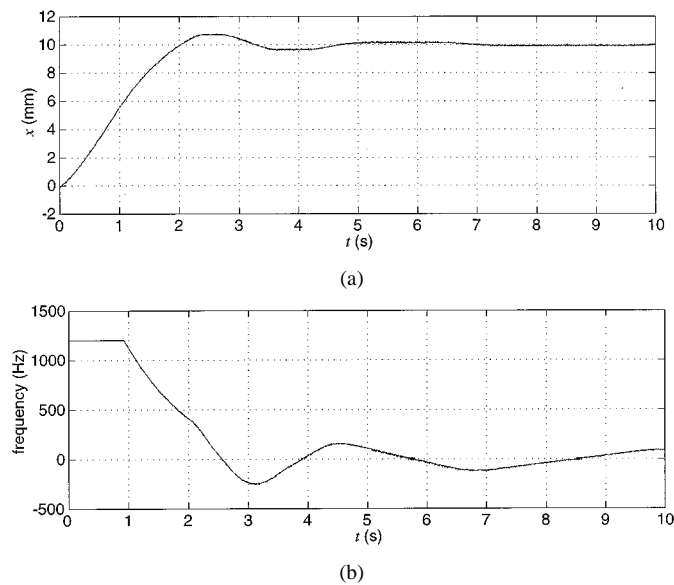


Fig. 12. 10-mm closed-loop step response and its corresponding frequency input with PI frequency control with the fixed phase current of 25 A.

VI. CONCLUSION

We have developed a linear magnetostrictive motor with a laminated Terfenol-D slab as the moving part. With the Terfenol lamination, the operation frequency of the magnetostrictive motor has been increased significantly. This magnetostrictive actuator does not require bearings or other components with friction, suggesting its utility in precision positioning. The motor self-brakes and holds its position when unpowered, which is beneficial to many applications.

Unlike existing piezoelectric peristaltic actuators, the magnetostrictive motor presented herein utilizes traveling magnetic field by three-phase double-sided double-layer armatures. This prevailing design of the stators leads to reduction in fabrication cost, since it does not require high-precision tight-fit design. The actuator mechanical design is in an open structure in order to allow easy assembly and access to internal actuator components. Eight sets of Belleville spring washers guarantee uniform squeeze preload in spite of wear, thermal expansion, or motion of the Terfenol-D element.

We designed and constructed power and control electronics for the linear magnetostrictive motor. We successfully implemented real-time digital control and presented test results under various operational conditions. As other Terfenol-based magnetostrictive actuators, the linear magnetostrictive motor presented in this paper had showed rather large reactive power. We were successful in using a series-resonant capacitor to provide the necessary reactive power to the motor, resulting in a near-unity power factor; the reactive power was reduced by a factor of 20 and the power factor was improved from 0.352 to 0.989.

The magnetostrictive motor has demonstrated 12-mm/s speed at excitation frequency of 1600 Hz, and shown 140-N load capacity to date. The effective travel range of the present motor is 25 mm, which can be extended further. In addition to these performance achievements, we addressed and provided solutions to the major challenges associated with typical magnetostrictive actuators—high eddy-current loss, wear, and low power factor.

This extended-range linear magnetostrictive motor shows great potential in high-force density precision applications such as automotive actuators, robotics, and flight control surface actuators.

ACKNOWLEDGMENT

The authors wish to thank S. Askew, the technical point of contact at NASA Johnson Space Center, Houston, TX, for his technical support throughout this magnetostrictive motor development program. We appreciate valuable contributions of our colleagues at SatCon Technology Corporation, A. E. Barnett and D. Havenhill.

REFERENCES

- [1] L. Sandlund, M. Fahlander, T. Cedell, A. E. Clark, J. B. Restorff, and M. Wun-Fogle, "Magnetostriction, elastic moduli, and coupling factors of composite Terfenol-D," *J. Appl. Phys.*, vol. 75, no. 10, pp. 5656–5658, May 1994.
- [2] E. T. de Lacheisserie, *Magnetostriction: Theory and Applications of Magnetoelasticity*. Boca Raton, FL: CRC Press, 1993.
- [3] L. Kiesewetter, "The application of Terfenol in linear motors," in *Proc. 2nd Int. Conf. Giant Magnetostrictive Alloys*, ch. 7, 1988, p. 15.
- [4] J. M. Vranish, D. P. Naik, J. B. Restorff, and J. P. Teter, "Magnetostrictive direct drive rotary motor development," *IEEE Trans. Magn.*, vol. 27, pp. 5355–5357, Nov. 1991.
- [5] W. Wang and I. Busch-Vishniac, "A high precision micropositioner based on magnetostriction principle," *Rev. Sci. Instrum.*, vol. 63, no. 1, pp. 249–254, Jan. 1992.
- [6] F. Claeysen, N. Lhermet, R. Le Letty, and P. Bouchilloux, "Design and construction of a resonant magnetostrictive motor," *IEEE Trans. Magn.*, vol. 32, pp. 4249–4251, Sept. 1996.
- [7] J. P. Teter, M. H. Sendaula, J. Vranish, and E. J. Crawford, "Magnetostrictive linear motor development," *IEEE Trans. Magn.*, vol. 34, pp. 2081–2083, July 1998.
- [8] S. Ashley, "Magnetostrictive actuators," *Mech. Eng.*, vol. 120, no. 6, pp. 68–70, June 1998.
- [9] J. H. Goldie, M. J. Gerver, J. Kiley, and J. R. Swenbeck, "Observations and theory of Terfenol-D inchworm motors," in *Proc. SPIE 5th Annu. Int. Symp. Smart Structures and Materials*, vol. 3329, Mar. 1998, pp. 780–785.
- [10] J. L. Butler, *Application Manual for the Design of Etrema Terfenol-D Magnetostrictive Transducers*. Ames, IA: Edge Technologies, Inc., 1988.
- [11] F. Stillesjö, G. Engdahl, and A. Bergqvist, "A design technique for magnetostrictive actuators with laminated active material," *IEEE Trans. Magn.*, vol. 34, pp. 2141–2143, July 1998.
- [12] G. F. Franklin, J. D. Powell, and A. Emami-Naeini, *Feedback Control of Dynamic Systems*. Reading, MA: Addison-Wesley, 1986.



Won-Jong Kim (S'89–M'97) received the B.S. (*summa cum laude*) and M.S. degrees in control and instrumentation engineering from Seoul National University, Seoul, Korea, and the Ph.D. degree in electrical engineering and computer science from Massachusetts Institute of Technology, Cambridge, in 1989, 1991, and 1997, respectively.

In September 2000, he joined the Department of Mechanical Engineering, Texas A&M University, College Station, where he is currently an Assistant Professor. Following receipt of the Ph.D. degree, he was with SatCon Technology Corporation, Cambridge, MA, for three years. His teaching and research interests focus on analysis, design, and real-time control of mechatronic systems, and nanoscale engineering and technology.

Dr. Kim received the Grand Prize from the Korean Institute of Electrical Engineers' Student Paper Contest in 1988, and the Gold Prize for his doctoral work from Samsung Electronics' Humantech Thesis Prize in 1997. He was a semifinalist of the National Institute of Standards and Technology's Advanced Technology Program 2000 Competition. He is the holder of two patents on high-precision multidimensional positioning systems.



James H. Goldie was born in Boston, MA, in 1955. He received the B.S. degree in engineering and applied science from Yale University, New Haven, CT, and the S.M. degree in mechanical engineering from Massachusetts Institute of Technology, Cambridge, in 1977 and 1982, respectively.

From 1982 to 1988, he was first with Litton's Itek Optical Systems Division and later with Adaptive Optics Associates of United Technologies Optical Systems, where he worked on the optomechanical design of both large- and small-aperture optical systems with active wavefront correction. In 1989, he joined SatCon Technology Corporation, Cambridge, MA, where he has been Project Leader for a number of research and development programs, including new electric machines for actuation and power generation; the use of smart materials for noise/vibration suppression, sonar transducers, actuators, motors and a continuously variable transmission; and the application of micromachining to inertial sensors, energy storage devices, and power electronic components. He is co-inventor on two patents, one for a rotary magnetostrictive motor and one for a multi-air-gap motor.



Michael J. Gerver was born in New York in 1949. He received the Ph.D. degree in physics from the University of California, Berkeley, in 1977.

He was a Post-Doctoral Researcher in the Laboratory for Plasma Studies, Cornell University, from 1976 to 1979, and a Research Scientist in the Plasma Fusion Center, Massachusetts Institute of Technology, from 1979 to 1990. From 1990 to 2000, he worked on applications of Terfenol-D and other smart materials, motor and magnet design, magnetic shielding, and motion and vibration control, first at

SatCon Technology Corporation, and then as an independent consultant. Since 2000, he has been a Senior Scientist with GE Medical Systems, Haifa, Israel, working on MRI systems.



Jerome E. Kiley received the B.S. degree in mechanical engineering from Lafayette College, Easton, PA, and the M.S. degree in mechanical engineering from Worcester Polytechnic Institute, Worcester, MA, in 1993 and 1995, respectively.

Since 1996, he has been with SatCon Technology Corporation, Cambridge, MA, where he has worked on the development of new technology for electro-mechanical drives, actuators, and power-electronics modules. Through finite-element analysis and innovative closed-form techniques, he has provided advanced structural, dynamic, and thermal analysis and design of these electro-mechanical systems. His efforts have led to successful prototypes for extended-travel magnetostrictive motors, micromachined vibratory gyros, and a continuously variable transmission.



John R. Swenbeck was born in Everett, MA, in 1960. He graduated third in his class from Salem High Vocational School of Electronics, Salem, MA.

He joined the Electro Mechanical Division, Campbell Enterprises, where he maintained and updated a wide range of electromechanical equipment until 1994. He then became the Lead Technician of the Magnetics Department, SatCon Technology Corporation, Cambridge, MA, where he has led development of manufacturing procedures and test of a number of electromechanical devices, including high-current planar transformers, high-packing-factor coils, inductors, motors, and generators. Many of these devices are wound with Litz wire and include aggressive thermal management features such as liquid-cooled slots and end turns. He has extensive experience in fabrication of smart material-based prototypes, maintaining the critical mechanical interfaces that affect performance. These prototypes include extended-travel magnetostrictive linear motors, pumps for space-suit cooling, reaction mass actuators for noise/vibration cancellation, sonar transducers, and actuators for control of the boundary layer around an airfoil.

Mr. Swenbeck has received National Aeronautics and Space Administration awards for his work on a linear motor wing-tip shaker and a space-suit cooling pump.